Dynamics of Gas−Surface Interactions: Reaction of Atomic Oxygen with Chemisorbed Hydrogen on Tungsten

J. Ree,[†] Y. H. Kim,[‡] and H. K. Shin*

Department of Chemistry,[§] University of Nevada, Reno, Nevada 89557

Received: February 25, 1997; In Final Form: April 16, 1997[⊗]

The reaction of gas-phase atomic oxygen with hydrogen atoms chemisorbed on a tungsten surface is studied by means of classical trajectory procedures. Flow of energy between the reaction zone and the bulk solid phase is treated in the generalized Langevin equation approach. Most reactive events occur in small-impact-parameter collisions, in which the incident gas atom undergoes only one impact with the adatom, producing vibrationally excited OH radicals on a subpicosecond scale via the Eley−Rideal mechanism. Short-time calculations show that, in these collisions, the formation of the OH bond and subsequent dissociation of the H−surface bond occur in ~100 fs. A small fraction of reactive events occurs in a multiple-impact collision, forming a long-lived complex on the surface. As the impact parameter increases, both reaction probability and vibrational excitation decrease, thus producing a population inversion. The dissipation of reaction energy to the heat bath can be adequately described using a 10-atom chain with the chain end bound to the rest of the solid. The probability of OH(g) formation is not sensitive to the variation of surface temperatures between 0 and 300 K, whereas it rapidly rises with the gas temperature up to 1000 K, above which it remains nearly constant. A modified LEPS potential energy surface is used for the reaction zone interaction, whereas the framework of harmonic representation is used in modeling chain atoms.

I. Introduction

There has been a surge of both experimental and theoretical research activity in the field of gas−surface reactions in recent years.[1−3] Among such studies are direct collisions of gas-phase reactants with adsorbates on a metal surface, which are of the Eley−Rideal (ER) type. This mechanism is considered to be much less common than the Langmuir−Hinshelwood type (LH), in which reactions are believed to occur between chemisorbed species that are in thermal equilibrium with the surface. However, recent experiments[4−9] and calculations[10−18] show evidence of a number of gas−surface reactions occurring more or less directly as a gas-phase reactant interacts with an adsorbate. Thus, understanding the dynamics of gas−surface collisions is of fundamental importance in studying reactivity of such gas−surface systems. Hydrogen atoms chemisorbed on a tungsten surface is one of the most widely studied adatom systems.[4,5,7,10,11,13−15,17,19−24] Since chemisorption energies for H on a close-packed metal surface lie in the range 2−3 eV,[25,26] there can be a large amount of energy released in the reaction of energy-rich gas reactants with the adatom. For reactants such as hydrogen and oxygen, the bond formed between the gas atom and the adatom is about 4.6 eV, and the exothermicity is close to 3 eV, which distributes in various modes of the product state. Therefore, the H−metal surface is an attractive reactive site for producing highly excited molecules. The problem of such product excitation is important in studying any reaction. It is important to note that when such excited species are involved in subsequent steps, the reaction can proceed at an increased rate. Thus, in such reactions catalytic activity may have to be interpreted in terms of not only the traditional concept of surface site specificity but also the participation of energy-rich intermediates.

The gas atom to adatom collision is of primary importance in determining the overall reactivity. However, the reactivity is strongly influenced by the presence of many nearby surface atoms. The interaction of a gas atom with the adatom/surface system is in many ways similar to the extensively studied gas-phase A + BC type collision.[27,28] A major difference is that C is now a solid surface involving many atoms, so the mass of C is infinite. Through transfer of energy from the nascent gas atom···adatom bond to the adatom···surface vibration and in turn to the bulk solid phase, gas−surface reaction can take place efficiently. This is in contrast to gas-phase systems in which atoms do not recombine. That is, the adatom to surface interaction serves as a doorway for energy transfer between the gas atom···adatom complex and the surface. Therefore, an understanding of energy transfer between the newly formed gas atom···adatom bond and the weakened adatom···surface bond and energy redistribution among the various modes in the interaction system is a prerequisite for a detailed appreciation of reactive events that follow.

The purpose of this paper is to study the reaction of gas-phase oxygen atoms with hydrogen atoms chemisorbed on the (100) tungsten surface. In the O(g) + H(ad)/W(100) system, the pertinent interactions are those between the gas atom and the adatom, between the adatom and the surface, and between the gas atom and the surface. Since the gas atom is under the influence of forces exerted by surface atoms, the latter interaction can contribute significantly to reactivity. We will include top layer and body-centered cubic layer atoms of several unit cells in the interaction model. Furthermore, we will introduce a mechanism by which energy can transfer between the reaction zone and the bulk phase. A rigorous approach to study the reaction requires setting up a realistic potential energy surface and solving the equations of motion for both the reaction zone atoms and solid atom vibrations. We formulate a modified

* To whom correspondence should be addressed.

§ Theoretical Chemistry Group Contribution No. 1162.

† Present address: Department of Chemistry Education, Chonnam National University, Kwangju, Korea.

‡ Present address: Department of Chemistry and Center for Chemical Dynamics, Inha University, Inchon, Korea.

⊗ Abstract published in *Advance ACS Abstracts,* June 1, 1997.

S1089-5639(97)00699-3 CCC: $14.00

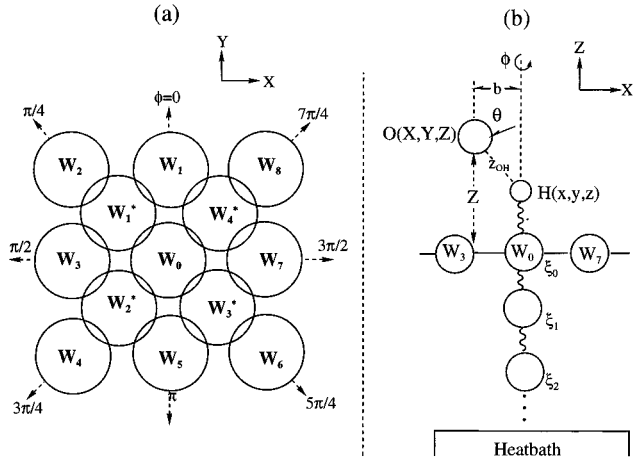

Figure 1. (a) Top view of the arrangement of surface atoms of four unit cells on the *XY* plane: circles with W_i are the (100)-plane atoms, and circles with W_j* are the bcc atoms. Eight atoms surrounding the center atom W_0 in the (100) plane are numbered $i = 1, 2, ..., 8$, and four bcc atoms ($j = 1-4$) are numbered $j = 1, 2, 3$, and 4. The azimuthal angle is measured counterclockwise around W_0, which is common to all four unit cells. (b) Collision coordinates; the side view (*XZ* plane) is shown. The chain atoms bound to the center atom (ξ_0) are numbered 1, 2, ..., *N*, with the vibrational coordinates $\xi_1, \xi_2, ..., \xi_N$.

London−Eyring−Polanyi−Sato potential energy surface and employ the molecular time-scale generalized Langevin equation approach, which is a fusion of the gas-phase trajectory method with the theory of generalized Brownian motion.[29−32] While we are mainly concerned with the reaction taking place at the gas temperature (T_g) of 1000 K and the surface temperature (T_s) of 0 K, the study will be extended further to consider the dependence of reaction probabilities on both T_g and T_s.

II. Interaction Potentials

The interaction coordinates and arrangement of W atoms in the body-centered-cubic (bcc) system are shown in Figure 1. We include eight (100) atoms (W_i, $i = 1-8$) and four bcc atoms (W_j^*, $j = 1-4$) of four unit cells, which surround the center atom W_0 in the model. The hydrogen atom is chemisorbed on the center atom, which is commonly shared by the four unit cells. The relative positions and elevations of these W_i and W_j^* atoms vary periodically around the center atom. While the overall gas−surface interaction is dominated by the O to H attraction, the interactions of the gas atom with these adjacent surface atoms are important since they may direct the gas atom toward the reaction site. The incident gas atom sees periodic features of the surface, so it is necessary to incorporate these features in the gas−surface interaction energy. A total of six degrees of freedom is needed to describe the motions of O and H atoms on the surface; they are O(*X*,*Y*,*Z*) and H(*x*,*y*,*z*). The O atom approaches a point on the *XY* plane of the surface with the impact parameter *b*. The topology of the *XY* plane around the center atom experienced by the gas atom can be conveniently described by the azimuthal angle ϕ, which ranges from 0 to 2π. This angle is related to the *X* and *Y* distances as $X = b \sin \phi$ and $Y = b \cos \phi$ for a given impact parameter *b*. During the approach, the gas atom interacts with the adatom, and the angle between the O···H axis and the surface normal is represented by $\theta = \tan^{-1}[b/(Z - z_{HW_0})]$, where z_{HW_0} is the H···W_0 bond distance. Here the center atom W_0 is the top atom of the (N+1)-atom chain. This angle varies from 0 to $^1/_2\pi$. For the adatom coordinate (*x*,*y*,*z*), it is reasonable to assume the adatom to undergo vibration in the normal direction such that $z = z_{HW_0}$ and $x = y = 0$. Thus, the pertinent coordinates needed for the present collision system are *Z*, θ, ϕ, and z_{HW_0}, along with the ξ's, which describe the vibrational motions of the chain atoms linking the reaction zone to the heat bath (see Figure 1b). The O to H distance is determined by $z_{OH} = (Z - z_{HW_0})/\cos \theta$.

The main interaction of the collision system is that which operates between the O atom and the adatom. However, the gas atom also interacts with nearby surface atoms W_i and W_j^*. Figure 1a shows the presence of W_i atoms at $\phi = {}^1/_4(i - 1)\pi$ and W_j^* atoms at $\phi = {}^1/_4(2j - 1)\pi$. The O-to-$W_i$ and O-to-W_j^* distances are

$$z_i = \{z_{OH}^2 + g_i^2 + c_i z_{OH} z_{HW_0} \cos\theta - 2 d_{WW} z_{OH} \sin\theta \cos[{}^1/_4(i-1)\pi - \phi]\}^{1/2}, \quad i = 1-8 \quad (1a)$$

$$z_j = \{z_{OH}^2 + g_0^2 + {}^1/_2 d_{WW}^2 + 2 z_{OH} g_0 \cos\theta - 2^{1/2} d_{WW} z_{OH} \sin\theta \cos[{}^1/_4(2j-1)\pi - \phi]\}^{1/2}, \quad j = 1-4 \quad (1b)$$

For the O-to-W_i interaction, $g_i = (z_{HW_0}^2 + d_{WW}^2)^{1/2}$ and $c_i = 2$ for i = odd, and $g_i = (z_{HW_0}^2 + 2 d_{WW}^2)^{1/2}$ and $c_i = 2^{3/2}$ for i = even. For the O-to-W_j* interaction, $g_0 = (z_{HW_0} + {}^1/_2 d_{WW})$. Here d_{WW} is the length of the side of the bcc unit cell. When $\theta = 0°$, the last term in each expression vanishes and the distances become independent of the azimuthal angle ϕ. During the collision, the gas atom becomes loosely bonded to the adatom, whereas the adatom to surface bond becomes weakened. When we refer to these weakly bound states, the corresponding distances will be designated by a dotted line as O···H and H···W_0 in the complex O···H···W_0. Then, the $\theta = 0°$ case represents the collinear configuration of O···H···W_0.

In addition to the surface atoms, we introduce a chain of W atoms that couples the reaction zone to the bulk phase and thus serves as a doorway for energy flow between the reaction zone and the bulk. The chain atoms ($n = 1 - N$) are linked to the center atom ($n = 0$), and their vibrational coordinates are denoted by $\xi_1, \xi_2, ..., \xi_N$; the coordinate of the center atom is ξ_0 (see Figure 1b). The motions of these chain atoms are responsible for dissipation of part of the reaction energy into the bulk solid phase. Thus, the chain is considered to provide a simple quasiphysical picture of energy flow between the reaction zone and the heat bath. All these *N*-chain atoms and W_i, W_j^* surface atoms interact directly with the gas atom. Thus, we consider that these atoms and the reaction zone atoms (O,H,W_0) constitute the *primary* system. We then designate the remaining infinite number of solid atoms as *secondary* atoms. It is certainly interesting to consider additional chains which begin with adjacent W_i and W_j^* surface atoms, but energy dissipation through such chains is far less efficient than that through the *N*-chain atoms which are directly bound to the center atom W_0. Secondary atoms influence the dynamics of the primary system through dissipative and stochastic force terms. These two terms balance, according to the fluctuation−dissipation theorem, so that the proper temperature is maintained in the primary zone.[31,32] Thus, we reduce the original many-body problem to a manageable size, which includes three reaction zone atoms, 12 surface atoms, and *N* chain atoms, where *N* is typically about 10.[18] Here, the chain portion replaces the bulk solid with a fictitious *N*-atom nearest neighbor harmonic chain 1, 2, ..., *N*, where the *N*th atom is bound to the rest of solid (the heat bath) and is subject to dissipative and stochastic forces.

The incident atom with collision energy *E* becomes trapped at the adatom site via inelastic interactions with the repulsive part of the O to H potential energy. The trapped atom undergoes an interaction with H on the surface, causing energy flow from the O···H vibration to the H···W_0 bond in the complex

O···H···W_0. When the H···W_0 bond gains sufficient energy, it dissociates to form OH in the gas phase, i.e., OH(g). Otherwise, O will rebound into the gas phase without reaction. The gas atom is in interaction with the adatom (H) and surface (S), which we characterize by chemisorption and physisorption types, respectively. We describe each atom−atom interaction energy in the reaction zone by the Morse function and model the interaction in the form of the London−Eyring−Polanyi−Sato (LEPS) type[10,21,33] as

$$U = Q_{OH} + Q_{HW_0} + Q_{OS} - [A_{OH}^2 + A_{HW_0}^2 + A_{OS}^2 - A_{OH}A_{HW_0} - (A_{OH} + A_{HW_0})A_{OS}]^{1/2} \quad (2)$$

For the O···H and H···W_0 interactions, the Coulomb and exchange terms are, respectively,

$$Q_k = {}^1/_4[D_k/(1+\Delta_k)][(3+\Delta_k)e^{(z_{k,e}-z_k)/a_k} - (2+6\Delta_k)e^{(z_{k,e}-z_k)/2a_k}] \quad (3a)$$

$$A_k = {}^1/_4[D_k/(1+\Delta_k)][(1+3\Delta_k)e^{(z_{k,e}-z_k)/a_k} - (6+2\Delta_k)e^{(z_{k,e}-z_k)/2a_k}] \quad (3b)$$

where k = O···H or H···W_0. In the exponential part, the subscript "e" represents the equilibrium distance of the atom pair indicated: See Table 1 for the values of these and other constants.[11,17,34−36] We note that $(Q_k + A_k) = D_k[e^{(z_{k,e}-z_k)/a_k} - 2e^{(z_{k,e}-z_k)/2a_k}]$, which is simply the potential energy of k in the Morse form. Therefore, the O−H and H−W_0 energies can be expressed as $E_{v,k} = (Q_k + A_k) + {}^1/_2 m_k \dot{z}_k^2$, where m_k is the reduced mass of the kth pair. Since the coordinate of the center atom W_0 is displaced by ξ_0 from its equilibrium position, we take the displacement of H···W_0 from the equilibrium bond distance $z_{HW_0,e}$ to be $(z_{HW_0,e} - z_{HW_0} - \xi_0)$ and use it in the exponents of Q_k and A_k for the H···W_0 interaction as $\exp[(\xi_0 + z_{HW_0} - z_{HW_0,e})/a_{HW_0}]$. For the O−surface physisorption interaction, we have many O-to-W_i and O-to-W_j^* terms. One of them is the gas atom to the normal direction of the surface and determines the collision trajectory Z, and the rest represents the gas to 12 surface atom interactions ($i = 1-8$, $j = 1-4$). Thus, the modified Coulomb and exchange terms for the gas atom-to-surface atom interaction are

$$Q_{OS} = {}^1/_4[D_{OS}/(1+\Delta_{OS})]\{[(3+\Delta_{OS})e^{(Z_e-Z)/a_{OS}} - (2+6\Delta_{OS})e^{(Z_e-Z)/2a_{OS}}] + \sum_{i=1}^{8}[(3+\Delta_{OS})e^{(z_{ie}-z_i)/a_{OS}} - (2+6\Delta_{OS})e^{(z_{ie}-z_i)/2a_{OS}}] + \sum_{j=1}^{4}[(3+\Delta_{OS})e^{(z_{je}-z_j)/a_{OS}} - (2+6\Delta_{OS})e^{(z_{je}-z_j)/2a_{OS}}]\} \quad (4a)$$

$$A_{OS} = {}^1/_4[D_{OS}/(1+\Delta_{OS})]\{[(1+3\Delta_{OS})e^{(Z_e-Z)/a_{OS}} - (6+2\Delta_{OS})e^{(Z_e-Z)/2a_{OS}}] + \sum_{i=1}^{8}[(1+3\Delta_{OS})e^{(z_{ie}-z_i)/a_{OS}} - (6+2\Delta_{OS})e^{(z_{ie}-z_i)/2a_{OS}}] + \sum_{j=1}^{4}[(1+3\Delta_{OS})e^{(z_{je}-z_j)/a_{OS}} - (6+2\Delta_{OS})e^{(z_{je}-z_j)/2a_{OS}}]\} \quad (4b)$$

There are no data on the physisorption of oxygen atoms on the tungsten surface, but such interactions are characterized by a shallow potential well and large values of the range parameter a_k and equilibrium distance $z_{k,e}$. The information available for related metal surfaces suggests that D_{OS} is in the range 0.10−0.15 eV. For example, the well depth D for the physisorbed O_2/Ir is 0.14 eV.[37] Assuming the ratio $D_{diatom/surface}/D_{atom/surface} = 1.2$ to hold in this case,[38] we estimate $D_{OS} = 0.12$ eV and take $z_{OS,e} = 4$ Å and $a_{OS} = 0.4$ Å to reflect the characteristics of physisorption. We adjust the Sato parameters Δ_k such that the resulting potential exhibits reaction channels and minimizes the contribution of the activation energy barrier as well as the attractive potential well over all O-to-W_i and O-to-W_j* directions. The result is $\Delta_{OH} = 0.49$, $\Delta_{HW_0} = 0.54$, and $\Delta_{OS} = 0.55$. Figure 2 shows the potential energy surface calculated with these Sato parameters in the direction of $\theta = 0$.

TABLE 1: Interaction Parameters

interaction	i = O−H	H−W_0	O−surface
D_i (eV)[a]	4.624[34][b]	2.30[11,17]	0.12[d]
ω_i (cm^{-1})	3738[34]	1820[17]	
$z_{e,i}$ (Å)	0.970[34]	1.67[35]	4.0[d]
a_i (Å)	0.218[c]	0.306[c]	0.40[d]
$\Theta_D = \hbar\omega_D/k = 400$ K[36][e]			

[a] $D = D_0^0 + {}^1/_2\hbar\omega_0$, where D_0^0 is taken from the reference. [b] Parentheses include references. [c] Calculated from $a_i = (D_i/2\mu_i)^{1/2}/\omega_i$. [d] See text. [e] The Debye temperature is needed in using ω_{en}, ω_{cn}, Ω_n, and β_n given in ref 18.

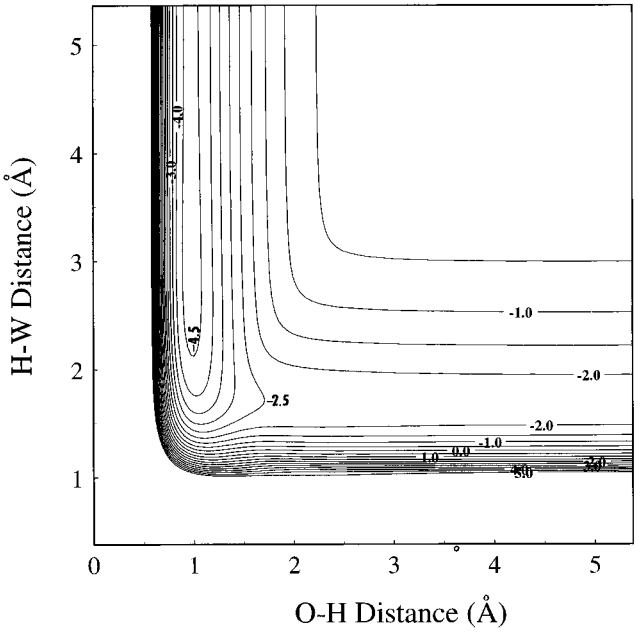

Figure 2. Potential energy contours in the directions of $\theta = 0$. The labeled contours are in eV and in a 0.5 eV interval.

In the present system, the dynamics of the O + H/W_0 interaction and in turn energy transfer from O···H to H···W_0 are influenced by inner atoms. We assume a set of (N+1) coupled equations of motion, including that for ξ_0, for a fictitious nearest neighbor collinear harmonic chain with the vibrational energy $V(\xi_n) = {}^1/_2 M\omega_{en}^2\xi_n^2$, where M is the mass of W and ω_{en} are the Einstein frequencies.[31] Because of the cross terms, the sum of solid interaction potential energies includes terms such as ${}^1/_2 M\omega_{\chi\nu}^2\xi_{n-1}\xi_n$, ${}^1/_2 M\omega_{\chi\nu+1}^2\xi_n\xi_{n+1}$, etc., where ω_{cn} are the coupling constants characterizing the chain. Thus, with the LEPS function given above, we can express the overall interaction potential in the form

$$U(Z,z_{HW_0},\theta,\phi,\{\xi_n\}) = \{Q_{OH} + Q_{HW_0} + Q_{OS} - [A_{OH}^2 + A_{HW_0}^2 + A_{OS}^2 - A_{OH}A_{HW_0} - (A_{OH} + A_{HW_0})A_{OS}]^{1/2}\} + \sum_n ({}^1/_2 M\omega_{en}^2\xi_n^{\,2} + {}^1/_2 M\omega_{cn}^2\xi_{n-1}\xi_n + {}^1/_2 M\omega_{c,n+1}^2\xi_n\xi_{n+1}) \quad (5)$$

where the notation $\{\xi_n\}$ denotes the set of chain atom coordinates (ξ_0, ξ_1, ξ_2, ... ξ_N) and Q_{OS} and A_{OS} represent the modified forms given by eqs 4a and 4b.

III. Equations of Motion

In the absence of interaction between the incident atom and the adatom (i.e., at a large distance from the surface), the angle θ is related to the impact parameter b as $\theta = \tan^{-1}[b/(Z - z_{HW_0})]$. When the O···H interaction sets in as the gas atom approaches the surface, θ now varies according to the angular velocity equation $d\theta(t)/dt = (2E/\mu)^{1/2}b/z_{OH}(t)^2$, where $z_{OH} = (Z - z_{HW_0})/\cos\theta$ and μ is the reduced mass of the collision system. However, once O···H is formed on the surface after the impact (or the *first* impact in a multiple-impact collision), θ now describes the rotational trajectory of O···H and its time evolution is governed by the equation of motion $I_{OH}d^2\theta(t)/dt^2 = -\partial U(Z,z_{HW_0},\theta,\phi,\{\xi_n\})/\partial\theta$, where I_{OH} is the moment of inertia. Therefore, the rotational trajectory $\theta(t)$ starts with $\theta(t_0) = \tan^{-1}\{b/[Z(t_0) - z_{HW_0}(t_0)]\}$ at initial time t_0 and evolves according to the angular velocity equation from the initial time t_0 to the time t_{FTP} (i.e., the time at the first turning point), and then according to the $I_{OH}d^2\theta(t)/dt^2$ equation from t_{FTP} to $+\infty$. In a multiple-impact collision, an active complex O···H···W_0 is formed after the first impact, so $I_{OH}d^2\theta(t)/dt^2$ describes the hindered rotational motion of O···H on the surface from the first turning point to the final turning point and then the rotation of the desorbing OH. A united set of the equations of motion for the reaction zone and N chain atoms can then be written as

$$\mu\ddot{Z}(t) = -\partial U(Z,z_{HW_0},\theta,\phi,\{\xi_n\})/\partial Z \quad (6a)$$

$$\mu_{HW_0}\ddot{z}_{HW_0}(t) = -\partial U(Z,z_{HW_0},\theta,\phi,\{\xi_n\})/\partial z_{HW_0} \quad (6b)$$

$$\dot{\theta}(t) = (2E/\mu)^{1/2}b/z_{OH}^2(t), \quad t_0 < t \le t_{FTP} \quad (6c)$$

$$I\ddot{\theta}(t) = -\partial U(Z,z_{HW_0},\theta,\phi,\{\xi_n\})/\partial\theta, \quad t_{FTP} < t < +\infty \quad (6c')$$

$$I\ddot{\phi}(t) = -\partial U(Z,z_{HW_0},\theta,\phi,\{\xi_n\})/\partial\phi \quad (6d)$$

$$M\ddot{\xi}_0(t) = -M\omega_{e0}^2\xi_0(t) + M\omega_{c1}^2\xi_1(t) - \partial U(Z,z_{HW_0},\theta,\phi,\{\xi_n\})/\partial\xi_0 \quad (6e)$$

$$M\ddot{\xi}_1(t) = -M\omega_{e1}^2\xi_1(t) + M\omega_{c1}^2\xi_0(t) + M\omega_{c2}^2\xi_2(t) \quad (6f)$$

$$M\ddot{\xi}_2(t) = -M\omega_{e2}^2\xi_2(t) + M\omega_{c2}^2\xi_1(t) + M\omega_{c3}^2\xi_3(t) \quad (6g)$$

. . . . . .

$$M\ddot{\xi}_{N-1}(t) = -M\omega_{e,N-1}^2\xi_{N-1}(t) + M\omega_{c,N-1}^2\xi_{N-2}(t) + M\omega_{c,N}^2\xi_N(t) \quad (6h)$$

$$M\ddot{\xi}_N(t) = -M\Omega_N^2\xi_N(t) + M\omega_{c,N}^2\xi_{N-1}(t) - M\beta_{N+1}\dot{\xi}_N(t) + Mf_{N+1}(t) \quad (6i)$$

where μ_{HW_0} is the reduced mass associated with the HW_0 bond. We integrate these equations from $t = t_0$ to $+\infty$ with eq 6c switched to eq 6c′ at $t = t_{FTP}$. Equations 6e−6i for $n = 0$, 1, 2, ..., N are the chain representations of many-body dynamics and correctly describe short-time (Einstein limit) processes. In the latter equations, ω_{en} and ω_{cn} are the short-time scale effective harmonic frequencies and Ω_N is the adiabatic frequency. Therefore, at short times the nth oscillator responds like an isolated harmonic oscillator with frequency ω_{en}, whereas Ω_N determines the long-time response of the heat bath. The friction coefficient β_{N+1} governs the dissipation of energy to the heat bath, which occurs a long time after the reaction.[18] The term $Mf_{N+1}(t)$ in eq 6i is governed by the fluctuation−dissipation theorem $\langle f_{N+1}(t)\, f_{N+1}(0)\rangle = (6kT_s/M)\beta_{N+1}\delta(t)$.[31] These friction and random forces are introduced in the last equation to mimic the effect of the heat bath. We stress that while many surface atoms are included in the model, we are considering a single chain with nearest harmonic interactions connecting the reaction zone to the bulk solid phase. Despite these simplifications, the approach of the effective equations of motion toward determining the coupling of the primary system to the heat bath is intuitive and treats the effects of the many-body problem on the gas−surface reaction in detail. Therefore, with computationally convenient friction kernels and fluctuating forces, eq 6 offers an approximate but realistic way of handling many-body coupling of the reactants to the solid atoms in the primary zone and then the primary zone to the heat bath.

Gas atoms were initially located above the surface at $z_{OS}(t_0) = 15$ Å. The gas atom approaches any location on the XY plane with b and E. We describe the initial direction of the gas toward the surface by $\phi = 2\pi l$, where l is a random number with a flat distribution in the closed interval (0,1). Next we sample collision energies at T_g in accordance with the Maxwell distribution function $f(E,T_g) \propto e^{-E/kT_g}$, instead of taking the average energy $\langle E\rangle$ at T_g. In sampling impact parameters, we note that d_{WW} is 3.03 Å,[39] whereas $z_{OH,e}$ is 0.970 Å,[34] so $1.5z_{OH,e}$ is very close to the halfway point between two adjacent surface atoms. (For convenience, we will express $z_{OH,e}$ by z_e throughout this section). Thus, we only consider gas atoms approaching the surface with an impact parameter in the range $0 \le b/z_e < 1.5$ and interacting with the H atom chemisorbed on the center surface atom W_0. The presence of other adatoms will not be considered in the present model. This situation corresponds to a low surface coverage where the interaction of the gas atom with other adatoms can be neglected. Otherwise, the interaction of the gas atom with other adatoms will have to be included in setting up the potential energy surface. Our results will show that reactive events are confined to the close range of the adatom under consideration such that the effect of other adatoms does not appear to be important.

The initial positions and momenta of the chain atoms, $\xi_n(t_0) = A_n \sin(\omega_{en}t_0 + \delta_n)$ and $\dot{\xi}_n(t_0) = \omega_{en}[A_n^2 - \xi_n(t_0)^2]^{1/2}$, where $A_n^2 = 2kT_s/M\omega_{en}^2$, and the phase δ_n were chosen for each trajectory at random from a Boltzmann distribution at T_s. The values of all pertinent coefficients ω_{en}, ω_{cn}, Ω_n, and β_n in the generalized Langevin part of the equations of motion are given elsewhere.[18] Random forces at each integration step were selected from a Gaussian distribution that rigorously satisfies the fluctuation−dissipation theorem. The initial condition for solving eq 6c is $\theta(t_0) = \tan^{-1}\{b/[Z(t_0) - z_{HW_0}(t_0)]\}$, and that for eq 6c′ is θ_{FTP}, which is the solution of eq 6c at $t = t_{FTP}$. The initial conditions for $Z(t_0)$ and $z_{HW_0}(t_0)$ are given elsewhere.[18] Note that $z_{HW_0}(t_0) \equiv z_{HW_0}(t_0,E^\circ_{v,HW_0},\delta_{HW_0})$, where δ_{HW_0} and E°_{v,HW_0}, are the initial phase and the initial energy of the adatom-to-surface atom vibration, respectively. We take the initial vibrational energy of 0.113 eV corresponding to the zero-point energy $^1/_2\hbar\omega_{HW_0}$. With these initial conditions, we integrate the equations of motion for the interaction energy described by eq 5 using an algorithm[40,41] with a time step of 0.30 fs or 1/30th the vibrational period of OH, the shortest period in the reaction system. Therefore, we can treat dynamics of gas−surface interaction and dynamics of chain atoms with equal rigor down to a subpicosecond scale with relatively modest computers. Note that $(Q_k + A_k)$ given in eqs 3a and 3b is simply the potential energy of k in the Morse form. For the most part of this study, we take the gas temperature T_g of 1000 K and the surface

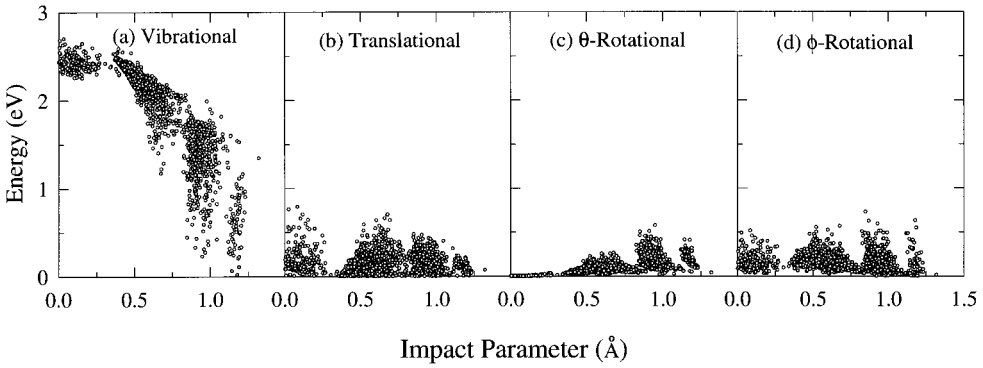

Figure 3. Dependence of (a) the vibrational energy, (b) the translational energy, (c) the θ-rotational energy, and (d) ϕ-rotational energy of the gas-phase product OH(g) on the impact parameter at $T_g = 1000$ K and $T_s = 0$ K.

temperature T_s of 0 K. However, we will extend the temperature ranges to $300 \leq T_g \leq 2500$ K and $0 \leq T_s \leq 300$ K to establish the temperature dependence of reaction probabilities. We sample 10 000 trajectories at each set of T_g and T_s in the impact parameter range of $0 \leq b < 1.5$ Å throughout this study.

During the collision, the gas atom is loosely bound to the adatom, whereas the adatom to surface bond becomes weakened, forming O···H···W_0. In each collision, the reaction is considered to have occurred and produced OH in the gas phase, if the O···H distance stabilizes to a well-defined vibrational motion of OH and the H···W_0 distance diverges. In a multiple-impact collision, the rebounding OH can be attracted back to the surface even after reaching a long distance from the surface. In such a collision, we follow the trajectory beyond the last turning point to establish the divergence of the H···W_0 distance. For this purpose, we extend the integration time to +50 ps. In some collisions, O···H produced on the surface can be stabilized to the trapped state permanently, i.e., OH(ad). We confirm this process by following such trajectories for 8 ns. Thus, collision events that occur in the present system can be classified as (i) those producing OH(g) in a single-impact collision on a subpicosecond scale, (ii) those producing OH(g) in a multiple-impact collision on a picosecond scale, (iii) those producing OH(ad) which are permanently trapped on the surface, and (iv) those producing no reaction.

IV. Results and Discussion

Before discussing the results, we consider the effects of chain length on the reaction to establish the optimum value of N for convergent results. For representative trajectories, energy transfer to the surface (E_s) is found to level off to a constant value for $N \geq 8$, indicating that we can do a realistic calculation of the gas−surface reaction with a relatively small number of chain atoms. Throughout this work, we will therefore use the 10-atom chain (i.e., $N = 9$). However, the effect of chain length on the model can be made arbitrarily precise by increasing N. The results show that energy transfer to the solid is small, indicating that in this reaction, where a light atom is adsorbed on a solid with a large Debye frequency ω_D, it is not easy to pump in energy from the reaction zone to chain atoms which are restored by a stiff spring. In the following sections A and B, we present the global aspects of the ensemble of all reactive trajectories. We then take representative trajectories of the ensemble for the details of collision dynamics in section C. Finally, a brief discussion on nonreactive collisions will be presented in section D.

A. Energy Distribution. In Figure 3, we show the distribution of the vibrational, translational, and rotational energies of OH between $0 \leq b < 1.5$ Å for all reactive events at $T_g = 1000$ K and $T_s = 0$ K. The figure shows several significant results on the dependence of these energies on the impact parameter. First, OH radicals produced in small-b collisions are vibrationally highly excited. Second, the vibrational energy decreases with increasing b, and OH formation ceases for $b > 1.3$ Å. Hydroxyl radicals produced in large-b collisions are only slightly excited or not excited at all. Third, there are many collisions in which significant conversion of vibrational to translational energy is evident. This energy conversion occurs at the final turning point where the trapped OH distributes its internal energy among various degrees of freedom. Rotational excitation in the θ-direction in small-b collisions is very small, but it becomes significant in large-b collisions. In the latter collisions, ϕ-rotational excitation is significantly larger. In small-b collisions, the torque developed is weak and O···H passes through the turning point and escapes before any substantial acceleration of θ can occur. In general, these rotational motions are ineffective in promoting OH(g) formation. On the other hand, in large-b collisions O···H is usually formed with an orientation close to side-on, in which case OH(g) desorbs with a significant amount of the θ-rotational energy. The comparison of the energy distributions shown in Figure 3 indicates that most of the energy released in the reaction is carried by the gas-phase OH in the form of vibration.

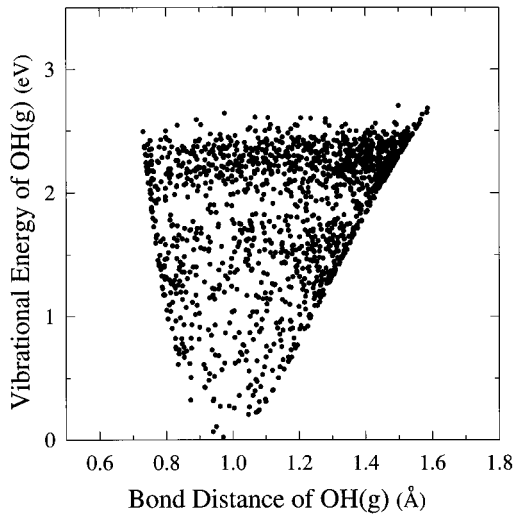

Figure 4. Plot of the OH(g) vibrational energy versus the OH(g) bond distance in the product state at $t = +50$ ps; $T_g = 1000$ K and $T_s = 0$ K.

Highly excited OH radicals undergo a large-amplitude vibration. A clear picture of such motion is seen in Figure 4, where the OH vibrational energy is plotted against the OH bond distance for all reactive collisions at $T_g = 1000$ K and $T_s = 0$ K. We follow all these reactive trajectories for a sufficiently long time of 50 ps, at which all product radicals are stabilized in their respective vibrational states. The OH bond distance lies within the range of its vibrational amplitude at a given

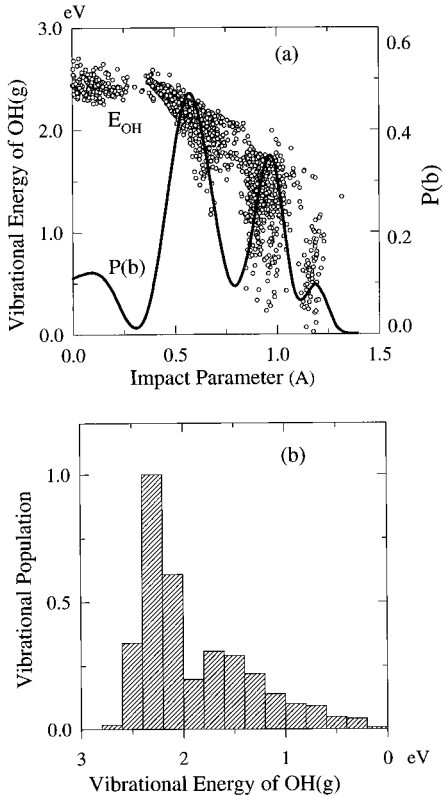

Figure 5. (a) Dependence of the reaction probability $P(b)$ on the impact parameter at $T_g = 1000$ K and $T_s = 0$ K. For comparison, the b dependence of the OH(g) vibrational energy is reproduced from Figure 3a. (b) Relative intensity of the vibrational population distribution for the product OH(g). The abscissa is displayed from the right to left to reflect the production of high $E_{v,OH}$ in small-b collisions.

vibrational energy. Figure 4 shows a clear picture of this range and the distribution of OH(g) bond distance. The distribution of bond distances for highly excited OH(g) radicals is very wide around the equilibrium value. There is a large concentration of vibrational amplitudes of high-lying OH(g) radicals near the outer turning point. The shape of the envelope boundary reveals a strong anharmonic vibration of excited OH radicals. This type of information is particularly useful in mapping *intra*molecular potential energy from experimental data. The measurement of vibrational energies and corresponding bond distances will determine the envelope, from which the intramolecular potential energy curve can be constructed.

To discuss the dependence of the vibrational energy of OH(g) on the impact parameter b in detail, we superimpose Figure 3a and the reaction probability at $T_g = 1000$ K and $T_s = 0$ K as shown in Figure 5a. The reaction probability is defined as $P(b) = N_R(b)/N(b)$, where $N_R(b)$ and $N(b)$ are the number of reactive trajectories forming OH(g) and the total number of trajectories sampled for a given value of b, respectively. The probability shows a structured dependence on b, taking several maximum values. This dependence demonstrates that the reaction takes place in different ranges of impact parameters and gives useful information about the origin of product excitation. The presence of such ranges has been noted already in the recombinative desorption of H_2 on Cu(111).[16] To discuss the b dependence, it is illustrative to imagine a "sphere of influence" with the radius z_e around the adatom. Near $b = 0$, where the incident gas atom is on top of the adatom and the O-to-H distance is close to z_e, vibrational excitation is very high, but the reaction probability is low. In such a collinear or near-collinear collision, the initial impact tends to form O···H in a compressed state with a large amount of energy accumulated in it. However, in such a compressed state, after turning the corner the O atom can rapidly rebound from the sphere of influence before O···H has had time to transfer its energy to the H···W_0 bond. Thus, only a small fraction of such collisions will survive during the round trip and produce OH(g). As the impact parameter increases, both reaction probability and vibrational excitation decrease, and the reaction finally ceases for $b > 1.3$ Å. At such a large b, the closest approach that the gas atom can make toward the adatom is when it is near the surface with the incident angle at 90° to the normal axis of H to W_0 shown in Figure 1b. In this case, the gas atom not only is very far from the adatom but is also in a repulsive interaction region of W_i and W_j* surface atoms. The variation of the vibrational energy and the reaction probability in the intermediate ranges of the impact parameter is particularly interesting. Figure 5a shows that the reaction is most efficient near $b = 0.5$ Å. In this b range, the incident atom can readily maintain its distance to the adatom close to the equilibrium value z_e. Another range of impact parameters occurs, where the reaction probability is again large, near $b = 1$ Å, which is very close to the equilibrium distance $z_e = 0.970$ Å. The probability in this range is not as high as that in the $b \cong 0.5$ case, but is far greater than that of the $b \cong 0$ case. Although the probability is still large, lower excitation begins to dominate in this large-b range. A much smaller fraction of reactive events with low excitation occurs near $b = 1.2$ Å. When $b > z_e$, O···H has a low vibrational energy and a long bond distance as it turns around the corner of the (final) turning point, but this configuration is unfavorable for O···H to stabilize as OH(g).

The results shown in Figure 5a indicate that the large number of highly excited OH radicals at one end of the vibrational energy spectrum and the small number of ground-state or low-excitation OH radicals at the other end create conditions for a vibrational population inversion (see Figure 5b). Figure 5b shows the distribution of all reactive trajectories over the range of OH vibrational energy from 0 to 3 eV. Here we have displayed the abscissa from $E_{v,OH} = 3.0$ eV to 0 eV to reflect the situation that small-b collisions produce highly excited OH, whereas large-b collisions produce unexcited or low-excitation OH. The maximum population occurs when $E_{v,OH} = 2.3$ eV, which is close to the $v = 5$ energy value calculated using the eigenvalue expression $E_{vib}(v) = hc\omega_e(v + {}^1/_2) - hc\omega_e x_e(v + {}^1/_2)^2$, with $\omega_e = 3738$ cm^{-1} and $\omega_e x_e = 84.88$ cm^{-1}.[34] A similar vibrational population inversion has been found in CO_2 produced from the reaction of oxygen atoms with chemisorbed CO on a platinum surface[18,42] and in H_2 produced from the recombination of gas-phase hydrogen atoms and chemisorbed hydrogen atoms on a tungsten surface.[17] Note that the total reaction cross section corresponding to $P(b)$ at $T_g = 1000$ K and $T_s = 0$ K is found to be $\sigma_R = 2\pi\int_{-\infty}^{\infty} P(b)b\ db = 0.859$ Å^2.

As noted in section II, the incident atom approaches the surface with the O-to-H direction at the angle $\theta = \tan^{-1}[b/(Z - z_{HW_0})]$ from the surface normal. When the O···H interaction sets in, however, θ varies according to the angular velocity equation $d\theta(t)/dt = (2E/\mu)^{1/2}b/z_{OH}(t)^2$ until $t = t_{FTP}$, where z_{OH} is dependent on the interaction potential. At the instant of the first impact, this equation gives the solution θ_{FTP}, which can be considered as the "true" incident angle toward the adatom. For all reactive collisions, the distribution of this angle varies approximately linearly with that of the impact parameter (see Figure 6a). Reactive events are confined to the angle range between 0 and 60°, and the linear relationship holds particularly well in small-b collisions. The appearance of four regions in the distribution reflects the corresponding peaks in Figure 5a. Figure 6a suggests that the dependence of $E_{v,OH}$ on θ_{FTP} should be similar to that on the impact parameter shown in Figure 5a. The smooth dependence of the vibrational energy on θ_{FTP} shown

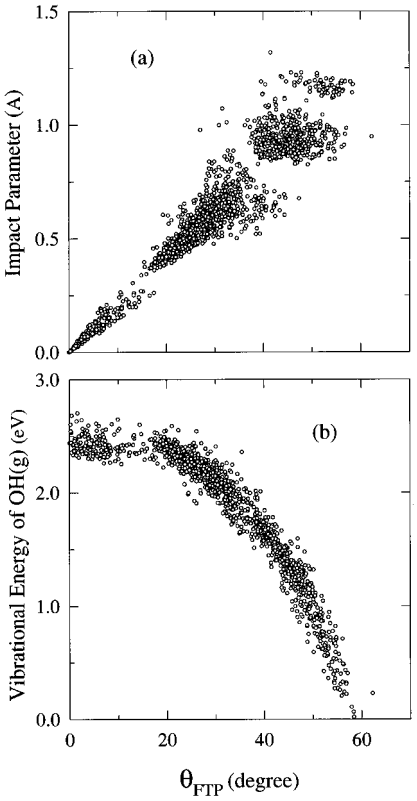

Figure 6. (a) Relationship between the incident angle at the first turning point θ_{FTP} and the impact parameter. (b) Dependence of the vibrational energy on θ_{FTP}.

in Figure 6b reflects this situation, as far less scatter occurs in $E_{v,OH}$ at a given θ_{FTP} than the $E_{v,OH}$ $-b$ plot shown in Figure 3a. This remarkable dependence indicates that the distribution of the vibrational energies of OH radicals is strongly dependent on the incident angle θ and furthermore, at a given incident angle, the vibrational energy of OH(g) is distributed over a narrow range. In a small-b collision, the incident atom will have to approach within the close range of the surface in order to have a large value of θ_{FTP}, but it is less likely for the incident atom to approach such a range in the presence of strong repulsive forces originating from many surface atoms. In these near head-on collisions, energy flow from O···H to H···W_0 can be efficient, as noted above, taking place in a short duration of the impact. On the other hand, in a large-b collision, the incident atom does not have to approach the close range of the surface in order to maintain a large θ_{FTP}. However, in the latter collision, which occurs in a distant region from the adatom, the reaction is less likely to occur.

B. Temperature Dependence of Reaction Probability. The above results are obtained for the reaction occurring at T_g = 1000 K and T_s = 0 K. We now look into the temperature dependence of reactive events. Figure 7 shows the distribution of reactive trajectories as a function of the vibrational energy for various gas temperatures. Here we keep the surface temperature at 0 K. To show the effect of gas temperature on the distribution, we have plotted the number of reactive trajectories as a function of the vibrational energy. (Note that Figure 5b shows the relative population.) Figure 7 shows that population inversion occurs at all gas temperatures considered. The general shape of the distribution of reactive trajectories remains essentially unchanged as the temperature is lowered from 2500 K to 1000 K. Below this temperature range, the distribution tends to become flat and the maximum shifts toward a lower vibrational energy.

The dependence of the reaction probability on the surface temperature is shown in Figure 8a, where the reaction probability

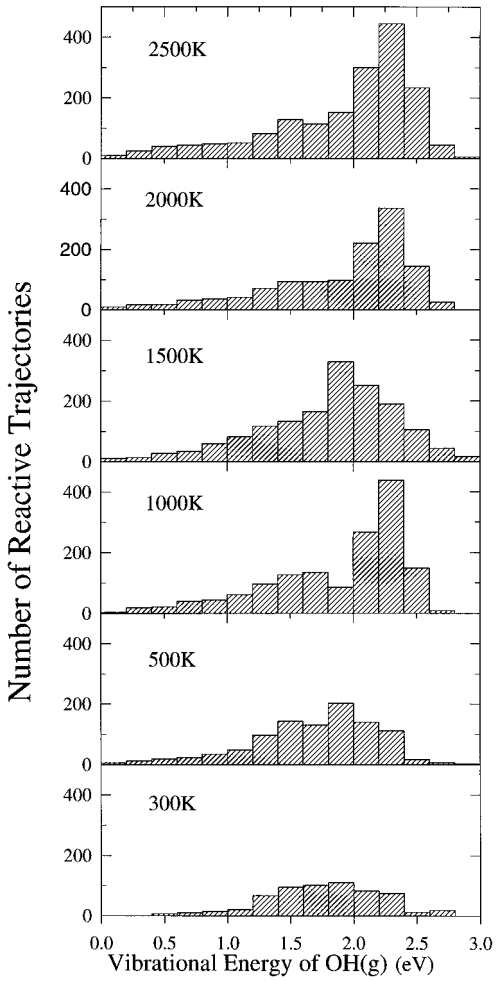

Figure 7. Vibrational population distribution for the product OH(g) at T_g = 300−2500 K and T_s = 0 K. The number of reactive trajectories is plotted as a function of $E_{v,OH}$. The total number of trajectories sampled at each temperature is 10 000.

is plotted from T_s = 0 to 300 K for the fixed value of T_g = 1000 K. The reaction probability plotted in this figure is defined as the ratio of the number of reactive trajectories to the total number sampled (10 000) over the entire range of impact parameters at a given T_g and T_s. It is then a total reaction probability and is different from $P(b) = N_R(b)/N(b)$ presented above (Figure 5a), which is the probability at a given impact parameter. Figure 8a shows that the total reaction probability is essentially independent of the surface temperature between 0 and 300 K, reflecting the situation that the reaction energy comes primarily from the incident atom, which is the essential feature of the ER mechanism. To understand such a weak temperature dependence, we note that the H···W_0 vibrational energy $\hbar\omega_{HW_0}$ is 0.226 eV and the fraction of adatoms in the H···W_0 vibrational energy state corresponding to the first excited state at T_s = 300 K is less than 0.02%. Thus, the contribution coming from excited H···W_0 states is not important. The weak T_s dependence of these probabilities indicates that the principal features of the reaction dynamics discussed above for T_s = 0 K remain unchanged. On the other hand, the dependence of the total reaction probability on the gas temperature is strong (see Figure 8b). For this plot, we have fixed T_s = 0 K and varied T_g from 300 to 2500 K. There is a significant increase in the reaction probability when the gas temperature is raised from 300 to 1000 K, but beyond this temperature range the probability increases only slightly. The reaction cross sections are found to be 0.385, 0.651, 0.859, 0.839, 0.844, and 0.802 Å^2 at T_g = 300, 500, 1000, 1500, 2000, and 2500 K, respectively, when the surface temperature is kept at 0 K. As in the reaction

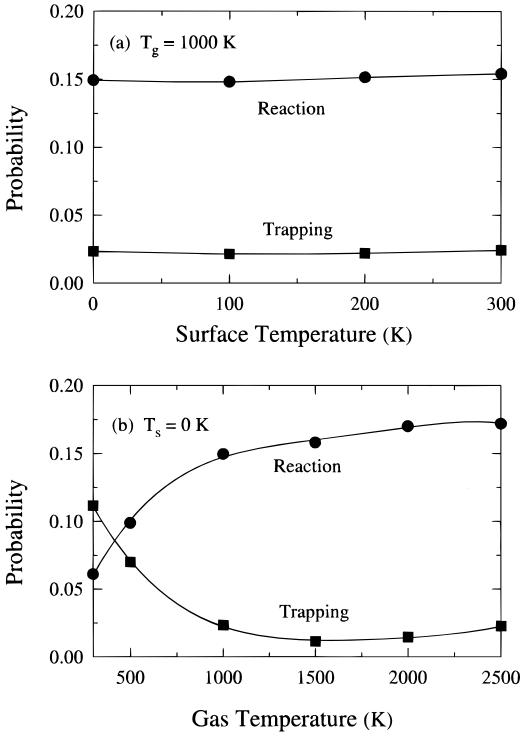

Figure 8. Temperature dependence of reaction and trapping probabilities. (a) Dependence on the surface temperature for the fixed gas temperature of 1000 K and (b) dependence on the gas temperature for the fixed surface temperature of 0 K.

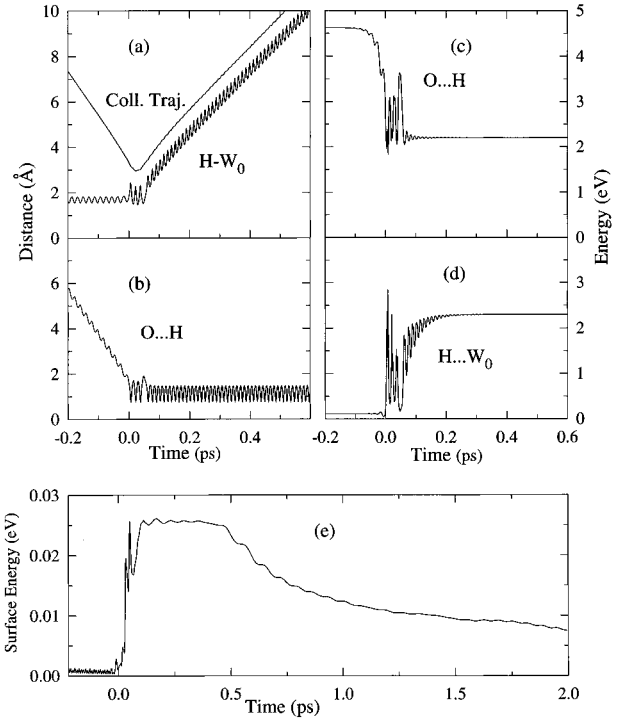

Figure 9. Reactive event representative of the ensemble of single-impact collisions. Plot of the evolution of (a) the collision trajectory and the H···W_0 distance, (b) the O···H distance, (c) the O···H vibrational energy, (d) the H···W_0 vibrational energy, and (e) the surface energy at $T_g = 1000$ K and $T_s = 0$ K. In part c, when OH is separated from the force field of the surface atoms, the O···H energy represents the vibrational energy of OH(g). In part d, after dissociation, the H···W_0 energy remains at 2.30 eV, the dissociation threshold.

probability, the temperature dependence of the cross section is weak between 1000 and 2500 K, but the cross section rises sharply as the gas temperature increases from 300 to 1000 K.

Also shown in Figure 8 is the trapping probability, which is defined as the ratio of the number of trajectories for permanently trapped OH(ad) to the total number sampled (10 000) over the entire range of impact parameters at a given T_g and T_s. This trapping probability represents the extent of OH(ad) radicals formed on the surface but unable to gain sufficient kinetic energy to escape into the gas phase. Although it is not shown in Figure 2, there is a shallow well in the exit channel, where the product OH can be trapped. The trapping probability is low and remains essentially constant when the surface temperature is raised from 0 K to 300 K at $T_g = 1000$ K (see Figure 8a). However, its dependence on the gas temperature is significant. As shown in Figure 8b, the trapping probability is significant at low gas temperatures, and in fact, it is larger than the probability of OH(g) formation at $T_g = 300$ K, where low-energy O···H can become trapped in the attractive well. The trapping probability decreases rapidly as the gas temperature increases and then remains nearly constant above $T_g = 1000$ K. It is interesting to note that the sum of the reaction and trapping probabilities is fairly constant over the entire gas temperature range, varying from 0.173 at $T_g = 300$ K to 0.195 at $T_g = 2500$ K.

C. Dynamics of Reactive Collisions. Nearly all reactive events occur in a single-impact collision, a direct reaction that is favored at high gas temperatures but is only very weakly affected by the surface temperature. At $T_g = 1000$ K and $T_s = 0$ K, nearly 98% of the reactive events occur at a reaction time of less than 1 ps in a single-impact collision following the "classic" ER mechanism of direct reaction between gas atoms and adatoms. The distribution of these single-impact collisions closely follows the logarithmic law of $\log[N(t_R)/N_0] \propto t_R$, with the slope yielding a rate constant of 4.60×10^{12} s^{-1}, where t_R is the reaction time, $N(t_R)$ is the number of single-impact trajectories, and N_0 is the total number of trajectories sampled. To define the reaction time t_R, we first confirm the occurrence of a reactive event by following the trajectory for 50 ps, which is a sufficiently long time for OH(g) to recede from the influence of surface interaction. Then we trace the reactive trajectory backward to find the time at which the H···W_0 separation has reached ($z_{HW_0,e}$ + 5.00) Å. We define this time as t_R. In a multiple-impact collision, it is the time at which the H···W_0 separation has reached this distance after the final turning point. Of the ensemble of 10 000 trajectories sampled in $0 \le b < 1.5$ Å at $T_g = 1000$ K and $T_s = 0$ K, 1494 have produced OH(g). Some of these reactive events occur with $t_R > 1$ ps, and nearly all of them involve two impacts. There are few trajectories that have t_R several picoseconds or longer. In such long-time events, the gas atom undergoes many impacts before forming OH in the gas phase. We consider the detailed dynamics of these collision processes in the following sections.

1. Single-Impact Collisions. To examine details of the collision dynamics, we select a trajectory that is representative of the ensemble of single-impact collisions at $T_g = 1000$ K and $T_s = 0$ K and plot the evolution of pertinent quantities in Figure 9. In Figure 9a we show the collision trajectory and H···W_0 distance. Note that the oscillatory variation of the H···W_0 distance after dissociation is due to the O···H vibration and has no significance. The evolution of the O···H distance is shown in Figure 9b. In order for the gas atom to interact with the adatom to form O···H on the surface and then desorb from the surface as OH(g) in a direct fashion, it must have sufficient kinetic energy to scatter inelastically from the repulsive part of the O-to-H interaction energy and be able to redirect sufficient energy along the H···W_0 vibration. The incident gas atom first decelerates, forming a loosely bound state O···H in the upper region of the potential well (i.e., slightly below the zero of the O···H interaction potential), and exchanges energy with the H···W_0 bond. OH(g) will form when the amount of energy transfer to the latter bond exceeds the dissociation threshold

D_{HW_0}. Otherwise, either the O atom rebounds from the surface (no reaction), or it becomes trapped on the adatom site permanently, forming OH in the adsorbed state (see sections IVC.3 and IVD). Figure 9a,b shows that the vibration of the loosely bound O···H bond is in near resonance with the vibration of the weakened H···W_0 bond during the period of a brief encounter near $t = 0$. This situation is shown by the three maxima of the H···W_0 vibration and the corresponding three minima of the O···H vibration in this period in Figure 9a,b.

Figure 9c,d shows energy flow between O···H and H···W_0 and the subsequent buildup of the H···W_0 energy toward the dissociation threshold. Thus, the outcome of each collision is dependent on the initial translational energy, the impact parameter, the strength of the H···W_0 bond, the initial phase of the H···W_0 vibration, and the process of energy transfer from O···H to H···W_0 in the complex. The O-to-H interaction energy, which starts out with D_{OH}, represents the vibrational energy of the short-lived O···H during the collision and then the vibrational energy of the desorbing product OH(g) after collision (see Figure 9c). On the other hand, the H-to-W_0 energy starts out with the initial vibrational energy of the HW_0 bond E°_{ν,HW_0} and then represents the vibrational energy of the weakened H···W_0 bond during the collision. When the bond dissociates, the H-to-W energy levels off to the constant value D_{HW_0}. The sharp rise and fall of these vibrational energies during the impact indicate an efficient flow of energy from the newly formed energy-rich O···H bond to H···W_0 in the complex O···H···W_0 on the surface as a result of a "strong collision" between the O and H atoms. The energy-rich O···H bond formed in the upper region of the potential well then descends to the lower region of the well. This process corresponds to a cascade of O···H transitions between the bound states of the potential. The evolution of $E_{\nu,OH}$ shown in Figure 9c indicates that the deactivation of this high-energy O···H occurs in a few steps, losing a large amount of energy ($\gg$kT) to the H···W_0 vibration at each step. Figure 9c,d clearly shows a near-resonant energy flow between these two bonds as the complex O···H···W_0 rapidly proceeds down the exit channel. During this process, the O···H interaction is still strongly attractive (see the variation of the energy contour near the OH distance of 1 Å in Figure 2), so that after the H···W_0 bond dissociation, a considerable amount of the initial O-to-H interaction energy remains in the vibration of the newly formed O···H bond as it moves toward the exit channel. This situation results in the production of a vibrationally excited OH(g) accompanied by some translational energy in the present exothermic reaction with an early-downhill surface.[43] The H-to-W_0 vibrational energy reaches its limiting value of 2.30 eV as the H···W_0 bond dissociates (see Figure 9d). Figure 9e shows the energy buildup in the solid chain on the O···H impact and its slow dissipation into the heat bath. All other plots for reactive events taking place in a single-impact collision look qualitatively like those shown in Figure 9a−e.

From short-time calculation, we can clock the dynamics of the OH formation and the H···W_0 dissociation during the lifetime of the complex O···H···W_0 in the reaction region (see Figure 10). A disturbance in the collision trajectory occurs near $t = 0$, where energy transfer to the H···W_0 begins. The discontinuities of the collision trajectory occurring between $t = 0$ and +60 fs correspond to the three minimum values of the O···H distance and in turn the three maximum values of the H···W_0 distance. In this reaction time range, the reaction coordinates O···H and H···W_0 are strongly coupled to each other, resonating at a frequency near 2100 cm^{-1}. A significant amount of acceleration of the H···W_0 distance occurs after turning the corner near $t = +60$ fs, where the H···W_0 excitation becomes strong. During this time interval, the O···H formed

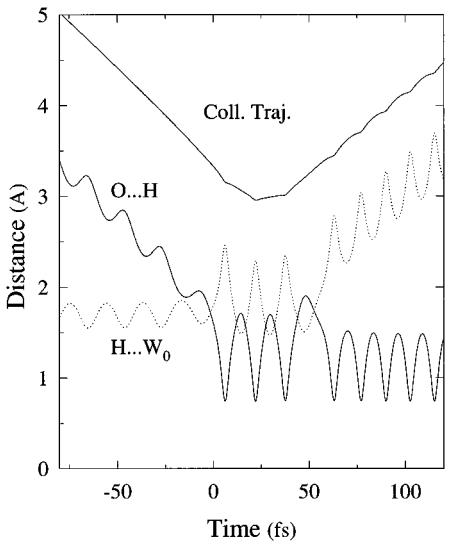

Figure 10. Short-time behavior of the collision trajectory, the O···H distance, and the H···W_0 distance at $T_g = 1000$ K and $T_s = 0$ K. Data in -80 fs $< t <$ 120 fs are taken from Figure 9a,b.

in the upper region of the potential well rapidly cascades down to the intermediate region, transferring its energy to the H···W_0 bond for bond dissociation. Here the O···H distance executes the final compression toward the surface, turning the attractive O···HW_0 interaction into a repulsive interaction of the OH···W_0. These processes and the production of the vibrationally excited OH take place in the short-time range of 60 fs. There is no evidence of OH attracted back to the surface beyond this range. In this reactive event, the displacement of the OH bond from its equilibrium value reaches a distance of 5 Å from the surface at $t_R = +370$ fs. Therefore, OH is completely out of the influence of surface attraction at $t_R = +370$ fs, but the decision for reaction is made long before this time.

The O···H attractive energy at the beginning of collision is 4.624 eV, and after dissociating the H···W_0 bond, the remaining energy and the collision energy for the representative trajectory considered in Figures 9 and 10 are distributed among various motions of the product OH as $E_{\nu,OH} = 2.199$ eV, $E_{t,OH} = 0.161$ eV, $E_{\theta,OH} = 0.085$ eV, and $E_{\phi,OH} = 0.205$ eV. The amount of energy transfer to the surface in this case is only $E_s = 0.025$ eV. This result indicates that nearly all the energy liberated in the reaction is carried by the gas-phase OH. The vibrational energy $E_{\nu,OH} = 2.199$ eV is very close to $E_{vib}(5) = 2.230$ eV calculated from the eigenvalue expression. It is important to mention the energy disposal for the entire ensemble of single-impact collisions. Nearly 98% of the reactive events occur in a single-impact collision, and the ensemble-averaged vibrational, translational, and rotational energies of all these single-impact collisions are 1.892, 0.322, and 0.140 eV, respectively. These values again show the dominant role of the vibrational motion in the sharing of reaction energy. The amount of energy transferred to the solid through the *N*-atom chain is only 0.024 eV. However, this does not mean that the effect of the chain is negligible or even uninteresting. In fact, the motions of the first several chain atoms are strongly coupled to the reaction zone through the H···W_0 bond, and energy transfer to these atoms can be large enough to deny the H···W_0 dissociation, when the H···W_0 vibration is near the dissociation threshold.

2. Double-Impact Collisions. Some reactive events occur in multiple-impact collisions on a picosecond scale. Most of these collisions involve double impacts. Although the number of such collisions is very small compared with that of single-impact collisions, these collisions represent an important class of gas−surface reactions. They are trapping-mediated reactive

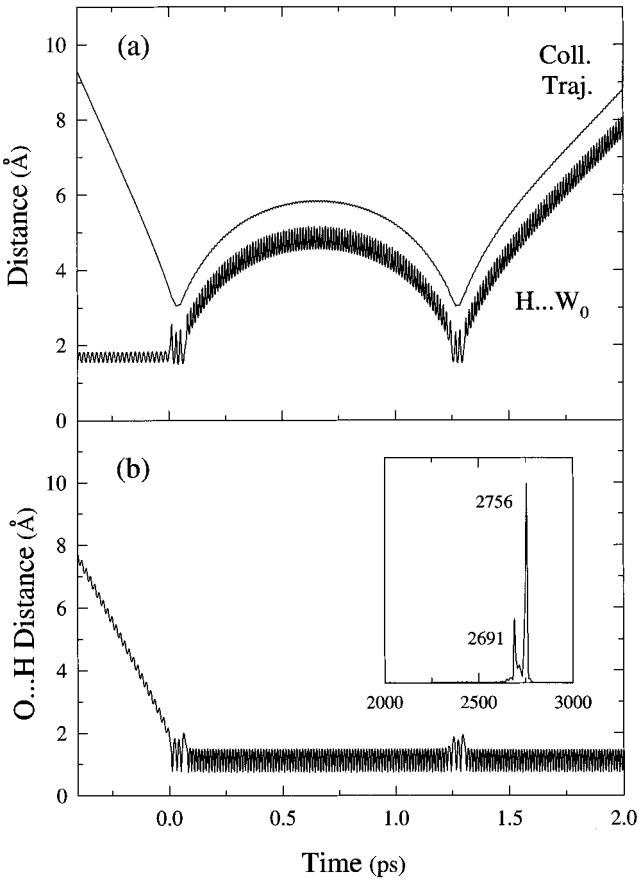

Figure 11. Reactive event representing double-impact collisions. (a) Collision trajectory and H···W_0 distance and (b) the O···H distance are shown at $T_g = 1000$ K and $T_s = 0$ K. The inset of part b is the power spectrum of the O···H vibration after the first impact. The main peak appearing at 2756 cm^{-1} is for the product OH(g), whereas the peak at 2691 cm^{-1} is the O···H vibration of the complex state O···H···W_0.

events, but unlike the Langmuir−Hinshelwood mechanism, the gas atom is now trapped on the adatom instead of an adjacent surface atom site. The lifetime of the complex O···H···W_0 formed on the surface in a multiple-impact collision is typically 2 ps. However, at $T_g = 1000$ K and $T_s = 0$ K, we find the lifetime as long as 12 ps. The gas atom forms an energy-rich O···H bond, and it has numerous opportunities to sample a suitable path for stabilization of the O···H bond and dissociation of the H···W_0 bond. The dynamics of such a reactive event that represents the ensemble of two-impact collisions at $T_g = 1000$ K and $T_s = 0$ K is shown in Figure 11. The lifetime of the trapped O···H in this double-impact collision is about 1.3 ps. The trajectory for the trapped portion of interaction is radically different from the single-turning-point (STP) trajectory considered above. Figure 11a shows that the rebounding O···H spends a relatively long time near the apex of the barely trapped state—where the kinetic energy vanishes—and fails to escape. In this trapped state, O···H undergoes a well-organized vibrational motion (see Figure 11b) with the frequency 2691 cm^{-1}, which is slightly red-shifted from the 2756 cm^{-1} for OH produced in the gas phase.

The near-resonant variation of the O···H and H···W_0 distances at the first turning point shown in Figure 11a,b is very similar to that of the STP case. At the first impact, the gas atom becomes trapped in the upper region of the potential well and the O···H bond transfers a large portion of its energy to the H···W_0 bond, bringing the H···W_0 bond energy up to near the dissociation threshold of 2.30 eV (see Figure 12a,b). Efficient energy flow occurs between the O···H and H···W_0 bonds during this initial encounter, as in the one-impact case.

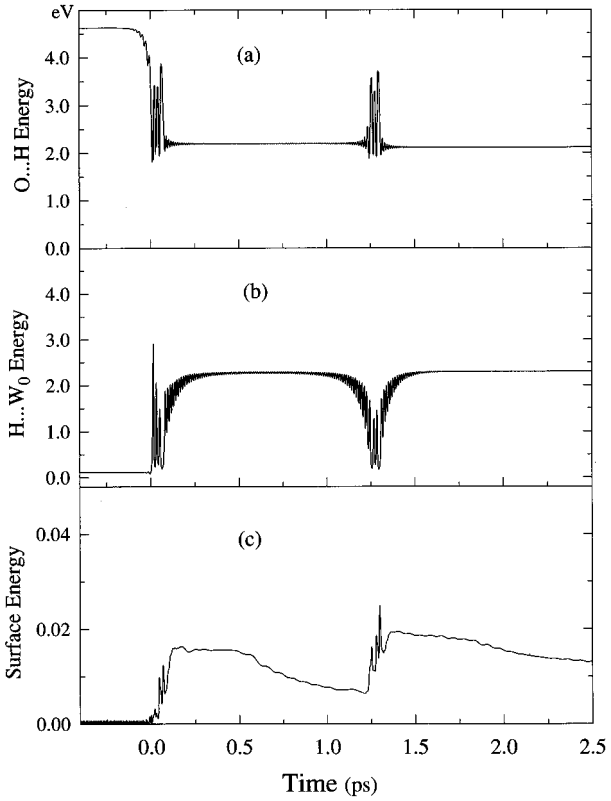

Figure 12. Double-impact collision displayed in Figure 11. (a) The O···H vibrational energy, (b) the H···W_0 vibrational energy, and (c) the surface energy. After the second impact, the O···H energy represents the vibrational energy of OH(g).

The O-to-H energy varies sharply during the first impact, and its variation is in resonance with that of the H-to-W_0 energy. The final peak of the O-to-H energy at the end of the impact represents the situation that as the O atom rebounds from H in the loosely bound O···H, there is an efficient flow of energy from O···H to H···W_0. Because of this energy loss to the H···W_0 bond, the O atom fails to escape from the adatom site. The peak height represents $E_{v,OH} = 3.8$ eV, but it decreases rapidly to 2.2 eV as the energy flows into the H···W_0 bond. The O···H motion is stabilized at $E_{v,OH} = 2.2$ eV for nearly 1 ps in the O···H···W_0 state until the second impact occurs. During this period, while O···H undergoes a highly regular vibration as shown in Figure 11b, the weakened H···W_0 bond vibrates at a large distance from the surface (see Figure 11a). This bond attempts to dissociate, but its energy is slightly below the threshold (see Figure 12b). Therefore, the dynamics near the first turning point is dominated by the approach of the gas atom to the adatom site (O→HW_0), whereas the dynamics near the second turning point (and all subsequent turning points in a multiple-impact collision) is dominated by the downward motion of O···H toward the surface (OH→W_0). At the second impact, the weakened H···W_0 bond gains a small amount of energy from the O···H motion, but this amount is sufficient to bring the H···W_0 energy just above the threshold. Figure 12a shows that the O···H motion transfers about 0.1 eV to the H···W_0 bond at the second impact. Although there is rapid intramolecular energy flow between O···H and H···W_0 during the second impact, the energy gained by the H···W_0 bond at the first impact is very close to the threshold energy, indicating that HW_0 gains essentially all the energy needed to dissociate during the brief period of the first round trip. The reaction completes near $t = +1.5$ ps, where OH desorbs with the vibrational energy 2.117 eV. Figure 12c shows the evolution of the surface energy. Although the magnitude is small, energy transfer to the surface chain atoms occurs rapidly at each impact,

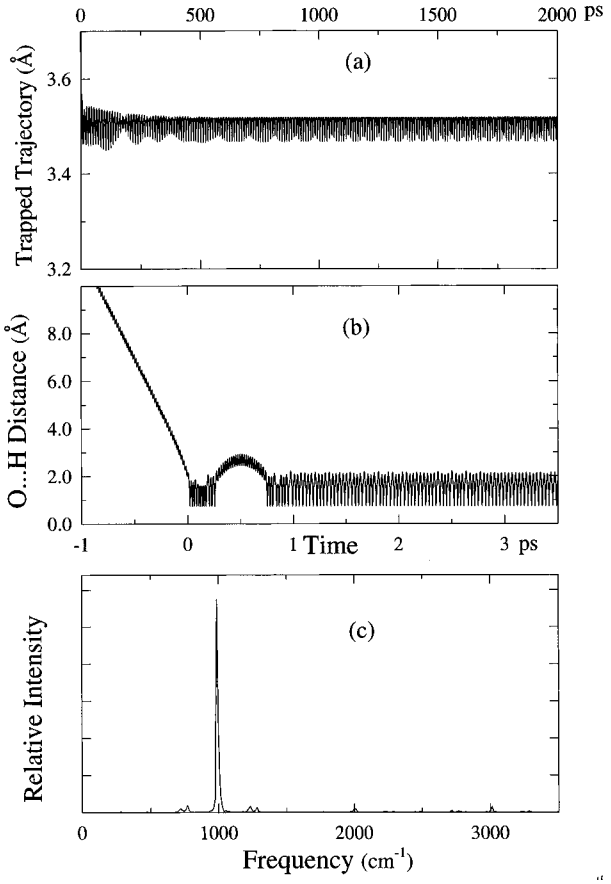

Figure 13. Permanently trapped case. (a) Long-time ($0 < t < 2$ ns) behavior of the trapped trajectory, (b) short-time ($-1 < t < 3.5$ ps) portion of the O···H distance of the trapped case, and (c) power spectrum of the OH(ad) vibration in the trapped state. $T_g = 1000$ K and $T_s = 0$ K. The time scale for part a is displayed at the top.

but dissipation into the heat bath is very slow, as in the single-impact case considered in Figure 9c.

3. Adsorbed OH. A significant fraction of gas atoms are trapped on the surface at lower temperatures. We have followed many such trajectories and found that they are trapped even at times as long as $t = +8$ ns. Both O···H and H···W_0 bonds in such collisions are found to undergo highly regular vibrational motions over the entire period, suggesting no likelihood of the H···W_0 bond dissociating at a later time. Therefore, we consider such O···H to be permanently trapped (or adsorbed) on the surface. As shown in Figure 8, the trapping probability is as large as 0.112 at $T_g = 300$ K and $T_s = 0$ K, whereas the reaction probability is only 0.061. As the gas temperature increases, the probability decreases rapidly. At $T_g = 1000$ K, it is only 0.023. The evolution of the trapped trajectory for 2 ns at $T_g = 1000$ K and $T_s = 0$ K is shown in Figure 13a. Figure 13b shows the evolution of the O···H distance during the early stage of trapping. The vibrational frequency of O···H in the trapped state shows a well-defined peak of 987 cm^{-1}, indicating that O···H is stabilized to OH(ad) in a highly excited state (see Figure 13c). This localization of the reaction energy in the vibrational motion of OH(ad) prevents the H···W_0 bond from gaining sufficient energy for dissociation.

D. Nonreactive Collisions. The total probability plotted in Figure 8 indicates that most incident gas atoms lead to no reaction. The data show that 83% of all trajectories sampled are nonreactive at $T_g = 300$ K and $T_s = 0$ K. Even at a gas temperature as high as 2500 K, nonreactive collisions constitute 81% of all trajectories. The dynamics of an event representative of the ensemble of nonreactive collisions at $T_g = 1000$ K and $T_s = 0$ K is shown in Figure 14. The evolution of the O···H and H···W_0 distances is shown in parts a and b of Figure 14, respectively. Even in such nonreactive collisions, there is a rapid flow of energy buildup in the H···W_0 bond, as in the reactive cases considered above. However, at the final stage of the impact, the rebounding atom takes back essentially all the energy from the H···W_0 bond. During the impact, the variation of the three minima in the O···H distance is in resonance with the three maxima in the H···W_0 distance, and the correspondence between these peaks and the energy flow peaks is clearly seen in Figure 14c,d. Note that during the impact the decrease in the O···H energy is greater than the increase in the H···W_0 energy, and this difference is due to energy transfer from the O···H bond to other modes such as the frustrated translational and rotational motions of O···H on the surface. Note that the saw-toothed variation of the H···W_0 energy after collision is due to energy flow between the H···W_0 bond and the surface atoms.

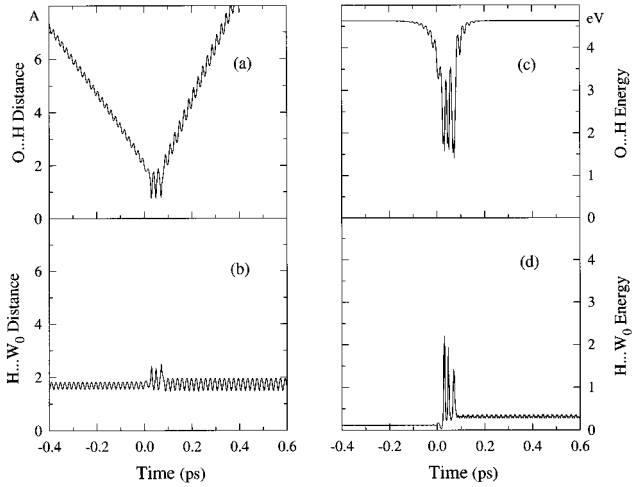

Figure 14. Nonreactive collision. Time evolution of (a) the O···H distance, (b) the H···W_0 distance, (c) the O···H vibrational energy, and (d) the H···W_0 vibrational energy at $T_g = 1000$ K and $T_s = 0$ K.

V. Concluding Comments

We have studied the reaction of O(g) + H(ad) on a tungsten surface by solving the effective equations of motion for the reaction zone atoms and the *N*-atom chain of the primary system. The model consists of the incident gas atom interacting with the adatom, 13 surface atoms, and the atom chain connecting the reaction zone to the bulk heat bath. We have used a modified LEPS potential energy function for the reaction zone interactions and harmonic representation for the vibrations of solid chain atoms. The reaction is treated at randomly sampled impact parameters, azimuthal directions, and collision energies.

Both the probability of OH formation and the probability of OH trapping are essentially independent of the surface temperature between 0 and 300 K at a given gas temperature. However, the probability of OH formation increases sharply when the gas temperature increases from 300 to 1000 K, but beyond this temperature range the probability remains nearly constant at 0.16. On the other hand, the extent of OH trapping increases significantly when the gas temperature is lowered below 1000 K. At a given surface temperature, the sum of the probabilities of OH(g) formation and OH(ad) trapping remains fairly constant over the gas temperature changes of 300 to 2500 K.

Nearly 98% of all reactive events occur in a single-impact collision via the Eley−Rideal mechanism. Even in such events, the collision produces a short-lived complex with the lifetime of about 100 fs or less, during which period there is an efficient flow of energy between the gas-to-adatom and adatom-to-surface

bonds. In multiple-impact collisions, reactions occur on a picosecond scale, during which the weakened adatom-to-surface bond undergoes a large-amplitude motion.

The energy liberated in the reaction deposits preferentially in the vibrational motion of the desorbing OH. This accumulation is particularly large in small-impact-parameter collisions. The reaction probability takes maximum values at some intermediate impact parameters between 0 and 1 Å. The formation of a large number of highly excited OH(g) in small-b collisions and a small number of low-excitation OH(g) in large-b collisions results in a vibrational population inversion, with the maximum population appearing at the vibrational energy corresponding to $v \cong 5$.

The amount of reaction energy transferred to the solid is small, and dissipation of the reaction energy into the heat bath is very slow compared with the time scale of the reaction. The model of the 10-atom chain subject to friction and random forces appears to be adequate for representation of the role of heat-bath atoms. The present procedure based on a union of the gas-phase equations of motions with generalized Langevin theory provides a useful framework for reducing the many-body dynamics problem of gas−surface reactions to equivalent few-body problems, revealing details of the dynamic behavior of the O(g) + H(ad)/W reaction.

Acknowledgment. The computational part of this research was supported by a NSF Advanced Computing Resources grant (CHE-890039P) at the Pittsburgh Supercomputing Center. J.R. and Y.H.K. gratefully acknowledge the financial support from Chonnam National University and Inha University, respectively.

References and Notes

(1) Rettner, C. T.; Ashfold, M. N. R., Eds. *Dynamics of Gas-Surface Interactions*; Royal Society of Chemistry: Thomas Graham House, Cambridge, England, 1991.
(2) Brivio, G. P.; Grimley, T. B. *Surf. Sci. Rep*. **1993**, *17*, 1.
(3) Somorjai, G. A. *Introduction to Surface Chemistry and Catalysis*; Wiley; New York, 1994.
(4) Hall, R. I.; Cadez, I.; Landau, M.; Pichou, F.; Schermann, C. *Phys. Rev. Lett.* **1988**, *60*, 337.
(5) Eenshuistra, P. J.; Bonnie, J. H. M.; Los, J.; Hopman, H. J. *Phys. Rev. Lett.* **1988**, *60*, 341.
(6) Schermann, C.; Pichou, F.; Landau, M.; Cadez, I.; Hall, R. I. *J. Chem. Phys.* **1994**, *101*, 8152.
(7) Kuipers, E. W.; Vardi, A.; Danon, A.; Amirav, A. *Phys. Rev. Lett.* **1991**, *66*, 116.
(8) Rettner, C. T.; Auerbach, D. J. *Science* **1994**, *263*, 365.
(9) Rettner, C. T.; Auerbach, D. J. *J. Chem. Phys.* **1996**, *105*, 8842.
(10) Elkowitz, A. B.; McCreery, J. H.; Wolken, G., Jr. *Chem. Phys.* **1976**, *17*, 423.
(11) Kratzer, P.; Brenig, W. *Surf. Sci.* **1991**, *254*, 275.
(12) Tully, J. C. *J. Chem. Phys.* **1980**, *73*, 6333.
(13) Shin, H. K. *J. Chem. Phys.* **1992**, *96*, 3330.
(14) Jackson, B.; Persson, M. *J. Chem. Phys.* **1992**, *96*, 2378.
(15) Jackson, B.; Persson, M. *Surf. Sci.* **1992**, *269*, 195.
(16) Jackson, B.; Persson, M. *J. Chem. Phys.* **1995**, *102*, 1078.
(17) Shin, H. K. *Chem. Phys. Lett.* **1995**, *244*, 235.
(18) Ree, J.; Kim, Y. H.; Shin, H. K. *J. Chem. Phys.* **1996**, *104*, 742.
(19) Tamm, P. W.; Schmidt, L. D. *J. Chem. Phys.* **1971**, *54*, 4775.
(20) Anders, L. W.; Hansen, R. S.; Bartell, L. S. *J. Chem. Phys.* **1973**, *59*, 5277.
(21) McCreery, J. H.; Wolken, G., Jr., *J. Chem. Phys.* **1977**, *66*, 2316.
(22) Barnes, M. R.; Willis, R. F. *Phys. Rev. Lett.* **1978**, *41*, 1729.
(23) Rettner, C. T.; Schweizer, E. K.; Mullins, C. B. *J. Chem. Phys.* **1989**, *90*, 3800.
(24) Xu, W.; Adams, J. B. *Surf. Sci.* **1994**, *319*, 45.
(25) Nordlander, P.; Holloway, S.; Norskov, J. K. *Surf. Sci.* **1984**, *136*, 59.
(26) Christmann, K. *Surf. Sci. Rep.* **1988**, *9*, 1.
(27) Shin, H. K. In *Dynamics of Molecular Collisions*; Miller, W. H., Ed.; Plenum; New York, 1976; pp 131−210.
(28) Yardley, J. T. *Introduction to Molecular Energy Transfer*; Academic; New York, 1980; Chapter 4.
(29) Adelman, S. A.; Doll, J. D. *J. Chem. Phys.* **1976**, *64*, 2375.
(30) Adelman, S. A. *J. Chem. Phys.* **1979**, *71*, 4471.
(31) Adelman, S. A. *Adv. Chem. Phys.* **1980**, *44*, 143.
(32) Tully, J. C. *J. Chem. Phys.* **1980**, *73*, 1975.
(33) Lee, C. Y.; DePristo, A. E. *J. Chem. Phys.* **1986**, *84*, 485.
(34) Huber, K. P.; Herzberg, G. *Constants of Diatomic Molecules*; Van Nostrand Reinhold: New York, 1979.
(35) Hugichi, I.; Ree, T.; Eyring, H. *J. Am. Chem. Soc.* **1957**, *79*, 1330.
(36) Gray, D. E., Ed. *American Institute of Physics Handbook*, 3rd ed.; McGraw-Hill: New York, 1972; p **4**−116.
(37) Kelly, D.; Verhoef, R. W.; Weinberg, W. H. *Surf. Sci.* **1994**, *321*, L157.
(38) Vidali, G.; Ihm, G.; Kim, H. Y.; Cole, M. W. *Surf. Sci. Rep.* **1991**, *12*, 133.
(39) Girifalco, L. A.; Weizer, V. G. *Phys. Rev.* **1959**, *114*, 687.
(40) *MATH/LIBRARY*; IMSL: Houston, 1989; pp 640, 1113.
(41) Gear, C. W. *Numerical Initial Value Problems in Ordinary Differential Equations*; Prentice-Hall: New York, 1971.
(42) Kori, M.; Halpern, B. L. *Chem. Phys. Lett.* **1984**, *110*, 223.
(43) Polanyi, J. C. *Acc. Chem. Res.* **1972**, *5*, 161.